

Effect of Different Loss Mechanisms in SiGeSn Based Mid-infrared Laser

© Vedatrayee Chakraborty*[¶], Bratati Mukhopadhyay*, P.K. Basu⁺

* Institute of Radio Physics and Electronics, University of Calcutta, Kolkata 700009, India

⁺ Electronics and Electrical Communication Engg. Dept. IIT Kharagpur, West Bengal 721302, India

(Получена 22 апреля 2014 г. Принята к печати 17 ноября 2014 г.)

We have analyzed the mid-infrared SiGeSn based Barrier-Well-Barrier Heterostructure and calculated the transparency carrier density and corresponding current density for the structure. The effects of different loss mechanisms like free carrier absorption, spontaneous recombination and Auger recombination processes on the transparency current density have been examined. It is shown that, the transparency current density increases significantly with the injected carrier density. Different scattering processes like acoustic phonon scattering and intervalley optical phonon scattering are taken into consideration for this analysis of free carrier absorption mechanisms.

1. Introduction

Si is one of the most widely studied materials in the history of civilization. In fact, the present day of information age could not come into existence in absence of electronics revolution brought about by the maturity of silicon based microelectronics. But there is no efficient light emission due to its indirect nature of band gap [1]. On the other hand, there is steady increase in the area of photonics, in the form of optical communication and networking, optical information processing, and consumer electronics based on light. The present day photonics relies on compound semiconductors and their alloys. Development of Si based active photonic devices remained a challenge over the last few decades. Over the last 10–15 years some significant milestones have been achieved [2–4]. The principal aim is naturally to realize efficient light emitters, modulators and photodetectors using Si and its alloys on Si substrate by using the existing microfabrication facilities, and to integrate all the devices and passive lightwave circuits. In all such attempts heterostructures formed by Si and its alloy with Ge, $\text{Si}_{1-x}\text{Ge}_x$ are the most studied material systems. The large amount of lattice mismatch between Si and Ge gives rise to strain and the critical layer thickness becomes a limiting factor.

Recently some novel ideas have been put forward [5–11] in the band structure engineering by using alloys of Si and Ge with Sn. Among the group-IV semiconductors, Ge is a potential candidate for an efficient light emitter. Although Ge is an indirect-bandgap material with its L valleys as the lowest conduction bands, the direct Γ -conduction band edge is only 134.5 meV above the L -conduction band edge at room temperature. This small energy difference between the direct- and indirect-conduction band edges implies the possibility of transforming Ge into a direct-bandgap semiconductor. One unique property of α -Sn is that the S -like Γ_7^- conduction band edge of α -Sn is situated below the P -like Γ_8^+ valence band edge, i.e. conduction band edge comes below the valence band edge which can effectively be

assumed as negative band gap. With this negative bandgap, alloying Ge with α -Sn can effectively reduce the energy difference between the Γ and L -conduction band edges to obtain direct-bandgap GeSn alloys for optoelectronic applications [5]. Such direct-bandgap behaviour has been observed experimentally [12–14]. In this way, the growth of direct bandgap $\text{Ge}_z\text{Sn}_{1-z}$ alloys has the potential to provide the gain medium for optoelectronic applications. As a result, the binary crystalline alloy $\text{Ge}_z\text{Sn}_{1-z}$ has received an extensive coverage in the scientific literature. But the ternary alloy $\text{Si}_x\text{Ge}_{1-x-y}\text{Sn}_y$ is a more thermodynamically stable material than binary [15] and it offers a wider range of device possibilities [16–19].

Moontragoon et al. [15] recently reported a practical design space for a variety of heterojunction (barrier-well-barrier) devices whose operating photon energy is in the 0.2 to 0.4 eV range. This implies that direct gap SiGeSn is suitable for a variety of mid-infrared photonic and optoelectronic applications. Previously the mid infrared QW laser and QW(W) laser structure and performance were proposed by [20–23] and the MQW laser structure using group IV material proposed by Chang et al. [24]. Chang et al. [24] has proposed a strain balanced $\text{Ge}_z\text{Sn}_{1-z}/\text{Si}_x\text{Ge}_y\text{Sn}_{1-x-y}$ QW structure which shows the gain at mid infrared region. However, to exploit fully the potential of ternary SiGeSn layers and to optimize the device performance, a need arises to understand the fundamental optoelectronic processes in these new materials. The study of the optical absorption of carriers in a semiconductor is important for the design of different optoelectronic devices. Amongst various factors contributing to the absorption of carriers, free carrier absorption (FCA) is an important component in the mid-infrared range. It is well known that, in the process of absorbing a photon, the electron must also absorb or emit a phonon or be scattered off by other imperfections in order to have both energy and wave vector conserved. The dependence of the FCA coefficient on photon frequency therefore depends strongly on the dominant scattering mechanisms. In the present work we address the problem of free carrier absorption loss in mid infrared laser structure using SiGeSn alloy as proposed

[¶] E-mail: vedatrayee_chakraborty@yahoo.co.in; bratmuk@yahoo.co.in

Table 1. The specifications of the hetero structures under consideration for lasing action (All transitions are referred to as Γ – Γ valley transitions)

Structure	Well	Barrier	Corresponding bandgaps (eV) $(E_{g\Gamma})_b$ to $(E_{g\Gamma})_w$	Strain	Valence band offset (eV) $(E_{v\Gamma})_b$ to $(E_{v\Gamma})_w$	Conduction band offset (eV) $(E_{c\Gamma})_b$ to $(E_{c\Gamma})_w$
A	$\text{Si}_{0.20}\text{Ge}_{0.45}\text{Sn}_{0.35}$	$\text{Si}_{0.546}\text{Ge}_{0.019}\text{Sn}_{0.435}$	0.2	Lattice matched	0.12	0.37
B	$\text{Si}_{0.25}\text{Ge}_{0.40}\text{Sn}_{0.35}$	$\text{Si}_{0.555}\text{Ge}_{0.022}\text{Sn}_{0.423}$	0.3	Lattice matched	0.1	0.30
C	$\text{Si}_{0.15}\text{Ge}_{0.621}\text{Sn}_{0.229}$	$\text{Si}_{0.637}\text{Ge}_{0.018}\text{Sn}_{0.345}$	0.4	Lattice matched	0.173	0.52

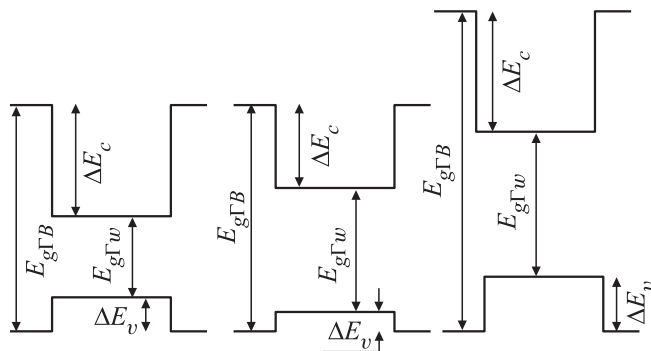
by Moontragoon et al. [15]. The hetero structure under consideration [15] in this work have lattice matched layer. So the heterostructures are strain free. There are two ways to make such heterostructure—either by the use of a strain relieved SiGeSn as buffer layer or to grow the first layer on Si with the thickness greater than the critical thickness.

We have selected three groups of compositions for SiGeSn well and barrier having the band gap of 0.2, 0.3 and 0.4 eV respectively. We calculated the reduction in gain due to FCA loss for these structures. The effect of spontaneous emission and Auger carrier loss are incorporated to determine the transparency current density. This paper has been arranged in the following manner. In the first section of the theoretical part, we have extracted the data of Moontragoon et al. [15] and proposed three well-barrier-well structures, and then the gain is calculated in the second section. The third section gives the detailed calculation of different loss mechanisms. This follows the results and discussions. Finally the paper ends with a conclusion.

2. Theory

2.1. Laser Structure

This section is completely based on the work of Moontragoon et al. [15]. Using empirical pseudopotential theory,


Figure 1. Band structure for the heterojunction laser for 0.2, 0.3 and 0.4 eV bandgap.

they calculated the direct (Γ) and indirect (L and X) band gaps of unstrained crystalline $\text{Si}_x\text{Ge}_{1-x-y}\text{Sn}_y$ over the entire xy composition range. They presented their results as energy contour maps on ternary diagrams along with a ternary plot of the predicted lattice parameters. We chose the well and barrier material composition in such a way that the well material has a direct gap, barrier material is lattice matched to the well, the two materials give type I confinement and the lowest of X or L valleys in both the well and the barrier materials is higher than the Γ valley in the well. The extracted compositions of Si and Sn for both well and barrier and the corresponding band gaps, conduction and valence band offsets are given in Table 1.

Fig. 1 shows the band structure for the heterojunction laser.

2.2. Calculation of Gain

In this section we have calculated the gain of the proposed heterostructure lasers. The barrier-well-barrier structure has been considered as a bulk structure and effect of quantum confinement has not been into consideration. So, the gain of the structure can be written as,

$$g(\omega) = \alpha(\hbar\omega) [f^e(E^e) - (1 - f^h(E^h))], \quad (1)$$

where

$$\alpha(\hbar\omega) = \frac{q^2(2m_r)^{1/2}}{2\pi\epsilon_0 c \eta m_0^2 \hbar^2} \frac{(\hbar\omega - E_g)^{1/2}}{\hbar\omega} \langle |P_{cv}^2| \rangle, \quad (2)$$

where m_e — effective mass for electrons, m_h — effective mass for holes, η — refractive index, ϵ_0 — permittivity of free space, c — velocity of light in free space, m_0 — free electron rest mass, \hbar — plank's constant, E_g — bandgap energy, $\langle |P_{cv}^2| \rangle$ — average of the square matrix element for transitions between Bloch states in the valence and conduction bands. We use the expression for $\langle |P_{cv}^2| \rangle$ for unpolarized light, which is

$$\langle |P_{cv}^2| \rangle = \frac{m_0^2 E_g (E_g + \Delta)}{3m_e (E_g + 2\Delta/3)}. \quad (3)$$

The term in the square brackets arises since the emission of photons in proportional to $f^e \cdot f^h$, while the absorption

process is proportional to $(1 - f^e)(1 - f^h)$. The difference of these terms appear in the above equation:

$$E^e = E_c + \frac{\hbar^2 k^2}{2m_e^*} = E_c + \frac{m_r^*}{m_e^* (\hbar\omega - E_g)}, \quad (4)$$

$$E^h = E_v - \frac{\hbar^2 k^2}{2m_h^*} = E_v - \frac{m_r^*}{m_h^* (\hbar\omega - E_g)}. \quad (5)$$

The occupation of electrons and holes in equilibrium is given by the Fermi level E_F . As excess electrons and holes are injected into the conduction and valance band respectively, occupation is given by quasi-Fermi levels, E_{Fn} and E_{Fp} .

2.3. Free carrier absorption

Free carrier absorption occurs when a material absorbs a photon and a carrier is excited from a filled state to an unoccupied state in the same band. Initially the electron is in a state \mathbf{k} in the conduction band it may go to the final state \mathbf{k}' in the same band only when a momentum scattering process is involved in addition to photon absorption. We considered two scattering process: acoustic phonon scattering and intervalley optical phonon scattering process. The transition rate can be written as [1]

$$W(\mathbf{k}) = \frac{2\pi}{\hbar} \Sigma |S_+ + S_-|^2 \delta(E_f - E_i), \quad (6)$$

where

$$S_+ = \frac{1}{\hbar\omega} \left[\langle \mathbf{k} \pm \mathbf{q} | H_{ep} | \mathbf{k} \rangle \langle \mathbf{k} | H_\lambda | \mathbf{k} \rangle - \langle \mathbf{k} \pm \mathbf{q} | H_\lambda | \mathbf{k} \pm \mathbf{q} \rangle \langle \mathbf{k} \pm \mathbf{q} | H_{ep} | \mathbf{k} \rangle \right]. \quad (7)$$

Where H_{ep} is the electron-phonon interaction potential. The optical matrix element is of the form

$$\langle \mathbf{k} | H_\lambda | \mathbf{k} \rangle = \frac{qA_0}{\hbar} \int U_k^* \exp(-i\mathbf{k}\mathbf{r}) (\epsilon\mathbf{p}) U_k \exp(i\mathbf{k}\mathbf{r}) d\mathbf{r}$$

and in the effective mass approximation this may be written as

$$\langle \mathbf{k} | H_\lambda | \mathbf{k} \rangle = \frac{qA_0}{\hbar} \epsilon_\lambda (\nabla_{\mathbf{k}} E) \left[n_\lambda + \frac{1}{2} \pm \frac{1}{2} \right]^{1/2} \quad (8)$$

considering only the stimulated emission and ignoring the spontaneous emission process. The absorption coefficient is calculated from the relation

$$\alpha_{fca} = \frac{\eta}{c} \frac{2\pi}{\hbar} \Sigma \{ |S_+|^2 + |S_-|^2 \} \delta(E_k - E_{k'} \mp \hbar\omega \mp \hbar\omega_q). \quad (9)$$

This equation is modified by including the probability $f(\mathbf{k})$ of having an electron at state \mathbf{k} and the probability $[1 - f(\mathbf{k}')]$ for not having an electron in state \mathbf{k}' . Considering phonon emission and absorption processes, the

following term should be inserted after $|S|^2$ in the above:

$$I_q = \left(n_q + \frac{1}{2} \mp \frac{1}{2} \right) f(\mathbf{k}) [1 - f(\mathbf{k}')] - \left(n_q + \frac{1}{2} \mp \frac{1}{2} \right) f(\mathbf{k}') [1 - f(\mathbf{k})]. \quad (10)$$

The + and - signs refer to phonon absorption and emission processes, respectively. Under equilibrium

$$n_{\lambda 0} \left(n_q + \frac{1}{2} \mp \frac{1}{2} \right) f(\mathbf{k}) [1 - f(\mathbf{k}')] - (n_{\lambda 0} + 1) \left(n_q + \frac{1}{2} \mp \frac{1}{2} \right) f(\mathbf{k}') [1 - f(\mathbf{k})] = 0, \quad (11)$$

where $n_{\lambda 0}$ is a photon number corresponding to a black body. Using this relation we can obtain

$$I_q = \frac{\sinh(\hbar\omega/2kT) [f(\mathbf{k}) - f(\mathbf{k}')] }{2 \sinh(\hbar\omega_q/2kT) \sinh[\hbar(\omega \pm \omega_q)/2kT]} = F_\pm(\omega, \omega_q) [f(\mathbf{k}) - f(\mathbf{k}')]. \quad (12)$$

Using the above relations we can calculate the absorption coefficient as

$$\alpha_{fca} = \frac{2V^2 \eta}{(2\pi)^6 c} \sum_{+-} \iint s(\mathbf{k}, \mathbf{k}') [f(\mathbf{k}) - f(\mathbf{k}')] F_\pm(\omega, \omega_q) \times \delta(E_{\mathbf{k}'} - E_{\mathbf{k}} - \hbar\omega \pm \hbar\omega_q) d\mathbf{k} d\mathbf{k}'. \quad (13)$$

Now, the effect of different scattering mechanisms can be determined considering the scattering matrix element for different scattering processes. The scattering matrix elements used for our calculation are given below:

For acoustic phonon scattering

$$\langle \mathbf{k}' | H_{ac} | \mathbf{k} \rangle = D_e \left[\frac{\hbar}{2V\rho\omega_q} \right]^{1/2} (\epsilon_q \cdot q) \left(n_q + \frac{1}{2} \pm \frac{1}{2} \right)^{1/2}. \quad (14)$$

Using Eqs (3), (5), (9) and (11) in Eq. (10) and performing the integrations, finally we get the absorption coefficient as

$$\alpha_{fca}|_{ac} = \frac{8}{3} \left(\frac{nq^2}{4\pi\epsilon_0} \right) \frac{\sqrt{(2/\pi)} \sqrt{(m_e kT)} D_e^2}{\hbar^3 \omega c \eta c_L} \times K_2 \left[\frac{\hbar\omega}{2kT} \right] \sinh \left[\frac{\hbar\omega}{2kT} \right], \quad (15)$$

where D_e is the effective deformation potential for acoustic phonon, n is the carrier concentration, η is the refractive index, ω is the photon frequency, c_L is the elastic constant along the principal axis of a valley and K_2 is a modified Bessel function of the second kind.

Table 2. Values of Different Parameters [26]

Parameters	Silicon(Si)	Germanium [Ge]	Tin[Sn]
Dielectric Constant	11.8	16
Lattice Constant	5.43 Å	5.657	6.48920
D_e	9.4450 eV	-5.3 eV
ρ	2.33 gm/c-c	5.32 gm/c-c	5.79 gm/c-c
s_L	$9 \cdot 10^5$ cm/sec	$5.4 \cdot 10^5$ cm/sec	$2.73 \cdot 10^5$ cm/sec
$D_1 = D_{\Gamma L}$	$4 \cdot 10^8$ eV/cm
$\omega_0 = \omega_{\Gamma L}$	$6.54 \cdot 10^{12}$ sec
Augur recombination coefficient	$1.4 \cdot 10^{-42}$ m ⁶ /sec ²	$2 \cdot 10^{-43}$ m ⁶ /sec

Similarly the absorption coefficient for intervalley optical phonon scattering can be written as,

$$\alpha_{inv} = \frac{n_r n e^2 D_{ij}^2 \hbar^2 \{n(\omega_0)[n(\omega_0) + 1]\}^{1/2}}{6c\pi^3/2(\hbar\omega_v)^3 \omega_0 m^* \epsilon_v \rho_m (k_B T)^{1/2}} \left[\frac{2m^*}{\hbar^2} \right]^{5/2} \times \sinh \left[\frac{\hbar\omega_v}{2k_B T} \right] \left[(\hbar\omega_+)^3 K_3 \left[\frac{\hbar\omega_+}{2k_B T} \right] + (\hbar\omega_-)^3 K_3 \left[\frac{\hbar\omega_-}{2k_B T} \right] \right], \tag{16}$$

where D_{ij} is intervalley optical phonon deformation potential, and ϵ_v is the permittivity. Here K_3 is the modified Bessel function of third kind.

All the expressions are derived considering constant spherical energy surfaces and parabolic bands. The fundamental contribution to the current density from spontaneous emission and Auger scattering losses were included phenomenologically to the total current density

$$J = J_{sp} + ed(CN_I^3), \tag{17}$$

where C is the Auger coefficient, N_I is the injected carrier density, J_{sp} is the current density from spontaneous emission phenomena has an expression given below [25],

$$J_{sp} = ed \int_0^\infty dv \left(\frac{n_B v}{\pi c} \right)^2 G(v) \left[\exp \left(\frac{h\nu - \mu_{eh}}{k_B T} \right) - 1 \right]^{-1}, \tag{18}$$

where, d is the active region thickness, k_B is the Boltzmann constant, and μ_{eh} is the electron-hole quasi-chemical potential energy separation taken to be transparency point in the gain spectrum.

3. Results and Discussion

The values of different parameters are given in Table 2. The values of different parameters are obtained for specific structures are obtained by linear interpolation. First, we considered unstrained $\text{Si}_x\text{Ge}_{1-x-y}\text{Sn}_y/\text{Si}_x\text{Ge}_{1-x-y}\text{Sn}_y$ (structure A) quantum well-barrier structure with band gap of 0.2 eV ($\lambda = 6.2\mu\text{m}$) [shown in Fig. 1]. We calculated the gain coefficient using eq. (1) and plotted in Fig. 2 with different carrier concentrations. The free carrier absorption coefficient is also calculated considering different scattering

mechanisms and shown by dotted lines in the same Figure. The free carrier absorption increases as expected with carrier concentration. As a result, the net gain decreases significantly with respect to the gain calculated without considering the effect of free carrier absorption, with the increasing carrier concentration as shown in Fig. 2. The similar calculations for other structures (B and C) as given in Table 1 for different band gaps (0.3 and 0.4 eV) are performed and the net gains are compared in Fig. 3. The transparency current density is calculated using the relating. $J_r = \frac{qdN_{tr}}{\tau_s}$ for structure A, is essential to start the lasing action in structure A. The active region width is taken as 300 Å. The transparency current density will increase due to the loss of Auger recombination and spontaneous recombination with increasing carrier density. The current due to Auger recombination and spontaneous recombination are calculated by Eqs (17) and (18) and the analytically calculated values are shown separately in Fig. 4. The sum of two current densities, i.e. $(J_{aug} + J_{sp})$ which causes significant increase in total transparency current density is shown in Fig. 4 by broken lines. As a result the total

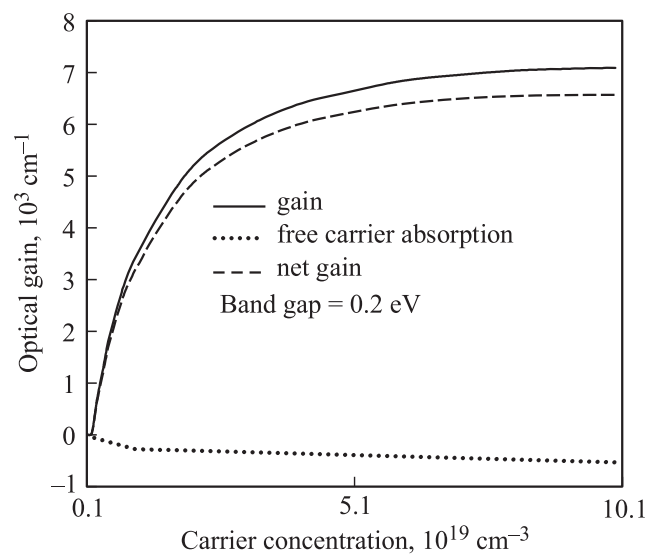


Figure 2. Variation of optical gain, free carrier absorption and the reduced gain/net gain with different carrier concentrations at 0.2 eV band gap for hetero structure A.

Table 3. Comparison among different structures

Structure of the model under consideration	Material used for modeling	Photon energy corresponding to the peak gain	Corresponding wavelength (λ)	Carrier concentration	Value of the peak gain coefficient
Heterostructure laser [our work]	$\text{Si}_{0.25}\text{Ge}_{0.40}\text{Sn}_{0.35}/\text{Si}_{0.555}\text{Ge}_{0.022}\text{Sn}_{0.423}$	0.31 eV	$4\ \mu\text{m}$	$4 \cdot 10^{18}\ \text{cc}$	950 cm
SiGeSn/GeSn/SiGeSn double heterostructure laser [27]	$\text{Si}_{0.15}\text{Ge}_{0.75}\text{Sn}_{0.1}/\text{Ge}_{0.94}\text{Sn}_{0.06}/\text{Si}_{0.15}\text{Ge}_{0.75}\text{Sn}_{0.1}$	0.77 eV	$1.6\ \mu\text{m}$	$4 \cdot 10^{18}\ \text{cc}$	95 cm
Quantum well structure [24]	$\text{Ge}/\text{Si}_{0.2}\text{Ge}_{0.7}\text{Sn}_{0.1}$	0.78 eV	$1.58\ \mu\text{m}$	$4 \cdot 10^{18}\ \text{cc}$	2000 cm

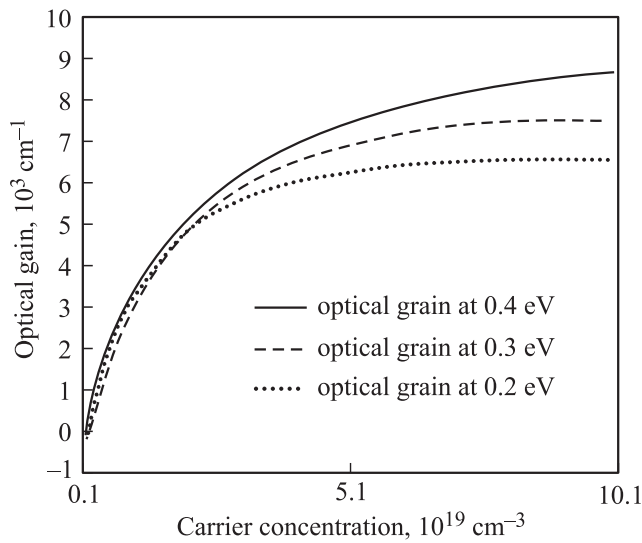


Figure 3. Comparison of net gain for structure A, B and C. The net gain is calculated considering different scattering mechanisms.

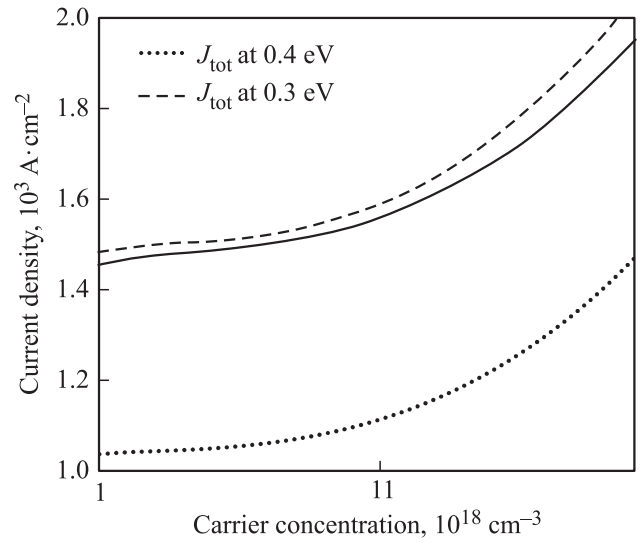


Figure 5. Comparison of total current density (with transparency current density) for structure A, B and C.

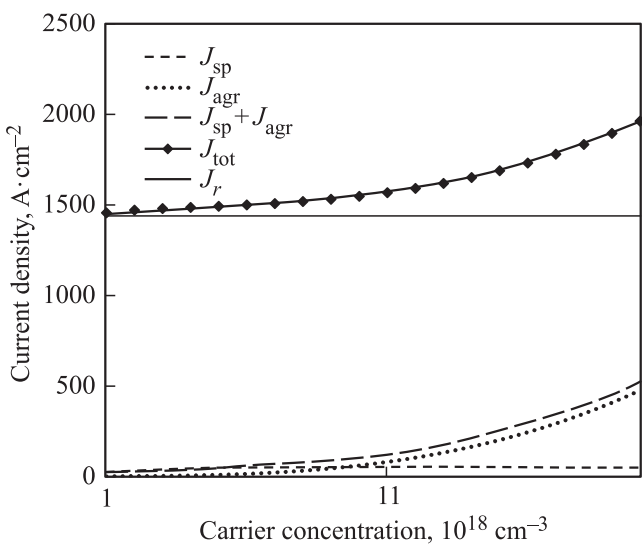


Figure 4. Variation of different current densities (Spontaneous recombination current density, Auger recombination current density, Total current density and transparency current density) with carrier concentration at 0.2 eV band gap.

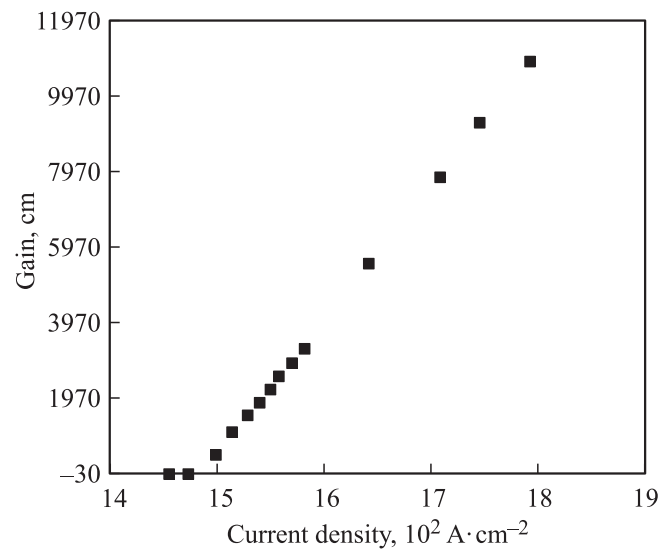


Figure 6. Variation f gain with the injection current density.

transparency current density (J_{tot}) increases with increasing carrier density as shown in Fig. 4. The comparisons of transparency current density (J_{tot}) for structure A, B and C are given in Fig. 5. In Fig. 6 optical net gain is plotted as a function of injection current density. In Table 3, our theoretical work is compared with the results of other researchers who worked on infrared lasers using the same materials.

Our model shows higher gain than that of a SiGeSn/GeSn/SiGeSn double heterostructure laser model [27] for same concentration while quantum well laser structure [24] shows higher value than that of our model at a fixed carrier concentration. Our proposed structure can be used in the near to mid infrared region with the wavelength of 4 μm .

4. Conclusion

We have studied the mid-infrared SiGeSn based structure and estimated the effective gain of the structure. It has been observed in our study that, due to free carrier absorption process the gain decreases; as for example with the structure having band gap of 0.2 eV, the gain decreases with an amount of $\sim 210/\text{cm}$ for carrier concentration of $7 \cdot 10^{18}/\text{cm}^3$. Similarly, the transparency current density cannot remain constant; rather it increases with the increase in the injected carrier density. The similar results are obtained for other structures having band gap of 0.3 and 0.4 eV. For 0.4 eV bandgap the lowest value of transparency carrier density is obtained. The Auger carrier losses and free-carrier absorption are incorporated to allow the estimation the net gain and current densities. The modified gain is useful for calculation of carrier induced refractive index change which plays a major role to predict the dynamical performance of laser and the quality of output beam.

The first author (VC) acknowledges financial support from the UGC, New Delhi, India sponsored Project Fellowship under its RESMS scheme.

References

- [1] P.K. Basu. *Theory of Optical Processes in Semiconductors: Bulk and Microstructures* (Oxford Univ. Press, Oxford, U.K., 2003).
- [2] G.T. Reed, A.P. Knights. *Silicon Photonics: An Introduction* (Wiley Interscience, N.Y., 2004).
- [3] M.J. Deen, P.K. Basu. *Silicon Photonics : Fundamentals and Devices* (Wiley, Chichester, U.K., 2012).
- [4] N. Izhaky, M.T. Morse, S. Koehl, O. Cohen, D. Rubin, A. Barkai, G. Sarid, R. Cohen, M.J. Paniccia. *IEEE Select. Top. Quant. Electron.*, **12**, 1688 (2006).
- [5] R.A. Soref, L. Friedman. *Superlat. Microstruct.*, **14**, 189 (1993).
- [6] R.A. Soref, C.H. Perry. *J. Appl. Phys.*, **69**, 539 (1991).
- [7] J. Taraci, J. Tolle, J. Kouvetakis, M.R. McCartney, D.J. Smith, J. Menendez, M.A. Santana. *Appl. Phys. Lett.*, **78**, 3607 (2001).
- [8] M. Bauer, C. Ritter, P.A. Crozier, J. Ren, J. Menendez, G. Wolf, J. Kouvetakis. *Appl. Phys. Lett.*, **83**, 2163 (2003).
- [9] J. Menéndez, J. Kouvetakis. *Appl. Phys. Lett.*, **85**, 1175 (2004).
- [10] P. Moontragoon, Z. Ikonc, P. Harrison. *Semicond. Sci. Technol.*, **22**, 742 (2007).
- [11] M. Virgilio, G. Grosso. *J. Phys. Condens. Matter*, **18**, 1021 (2006).
- [12] G. He, H.A. Atwater. *Phys. Rev. Lett.*, **79**, 1937 (1997).
- [13] H.P.L. de Guevara, A.G. Rodriguez, H. Navarro-Contreras, M.A. Vidal. *Appl. Phys. Lett.*, **84**, 4532 (2004).
- [14] R. Ragan, H.A. Atwater. *Appl. Phys. Lett.*, **77**, 3418 (2000).
- [15] P. Moontragoon, R.A. Soref, Z. Ikonc. *J. Appl. Phys.*, **112**, 073 106 (2012).
- [16] V.R. D'Costa, Y.-Y. Fang, J. Tolle, J. Kouvetakis, J. Menendez. *AIP Conf. Proc.*, **1199**, 39 (2009).
- [17] V.R. D'Costa, Y.-Y. Fang, J. Tolle, J. Kouvetakis, J. Menendez. *Thin Sol. Films*, **518**, 2531 (2010).
- [18] J. Kouvetakis, J. Tolle, J. Mathews, R. Roucka, J. Menendez. *ECS Trans.*, **33**, 615 (2010).
- [19] S. Bagchi, C.D. Poweleit, R.T. Beeler, J. Kouvetakis, J. Menéndez. *Phys. Rev. B*, **84**, 193 201 (2011).
- [20] N. Tansu, L.J. Mawst. *IEEE J. Quant. Electron.*, **39**, 1205 (2003).
- [21] I. Vurgaftman, J.R. Meyer, N. Tansu, L.J. Mawst. *Appl. Phys. Lett.*, **83**, 2742 (2003).
- [22] I. Vurgaftman, J.R. Meyer, N. Tansu, L.J. Mawst. *J. Appl. Phys.*, **96**, 4653 (2004).
- [23] W.W. Bewley, C.L. Canedy, C.S. Kim, M. Kim, C.D. Merritt, J. Abell, I. Vurgaftman, J.R. Meyer. *Opt. Express*, **20**, 3235 (2012).
- [24] G. Chang, S.W. Chang, S.L. Chuang. *Opt. Express*, **17**, 11 246 (2009).
- [25] W.W. Chow. *Appl. Phys. Lett.*, **100**, 191 113 (2012).
- [26] F.M. Armando, S. Fahy. *J. Appl. Phys.*, **109**, 113 703 (2011).
- [27] G. Sun, R.A. Soref, H.H. Cheng. *J. Appl. Phys.*, **108**, 033 107 (2010).

Редактор Т.А. Полянская